Journal of Applied Polymer Science

Preparation and Characterization of a Poly(methyl methacrylate) Based Composite Bone Cement Containing Poly(acrylate-*co*-silane) Modified Hydroxyapatite Nanoparticles

Minyu Rao, Qiangwei Su, Zhenzhen Liu, Peiqing Liang, Nan Wu, Changyun Quan, Qing Jiang
Biomedical Engineering Program, School of Engineering, Sun Yat-Sen University, Guangzhou 510006, China
M. Rao, Q. Su, and C. Quan contributed equally to this article.
Correspondence to: C. Quan (E-mail: quancy2010@163.com)

ABSTRACT: The purpose of this study was to study the mechanical properties of poly(methyl methacrylate) (PMMA)-based bone cement incorporated with hydroxyapatite (HA) nanoparticles after surface modification by poly(methyl methacrylate-*co*-γ-methacryloxypropyl timethoxysilane) [P(MMA-*co*-MPS)]. PMMA and P(MMA-*co*-MPS) were synthesized via free-radical polymerization. P(MMA-*co*-MPS)-modified hydroxyapatite (m-HA) was prepared via a dehydration process between silane and HA; the bone cement was then prepared via the *in situ* free-radical polymerization of methyl methacrylate in the presence of PMMA and P(MMA-*co*-MPS)–m-HA. Fourier transform infrared (FTIR) spectroscopy, ^{1}H-NMR, and gel permeation chromatography were used to characterize the P(MMA-*co*-MPS). Thermogravimetric analysis and FTIR were used as quantitative analysis methods to measure the content of P(MMA-*co*-MPS) on the surface of HA. The effect of the proportion of m-HA in the PMMA-based bone cement on the mechanical properties was studied with a universal material testing machine. A 3-(4,5-dimethylthiazol-2-yl)-2,5-diphenyltetrazolium bromide assay was also carried out to determine the cytotoxicity of the composite bone cement. The results showed that the surface modification of HA greatly improved the interaction between the inorganic and organic interfaces; this enhanced the mechanical properties of bone cement for potential clinical applications. © 2014 Wiley Periodicals, Inc. J. Appl. Polym. Sci. **2014**, *131*, 40587.

KEYWORDS: biomaterials; composites; mechanical properties

Received 12 October 2013; accepted 11 February 2014
DOI: 10.1002/app.40587

INTRODUCTION

Poly(methyl methacrylate) (PMMA) bone cement has been widely applied in the clinical treatment of bone injuries and artificial joint replacement/fixation because of its advantages, including its good mechanical properties and curing according to the shape of bone defect.[1,2] However, PMMA bone cement itself is bio-inert and unable to establish efficient integration between the host bone tissue and bone cement; this leads to inferior interfacial strength between the bone cement and the host bone tissue as well as the implant. Orthopedic implants would be loosened, and this would cause failure after a few years.[3,4] A large number of studies have been performed to improve the bioactivity of PMMA bone cement in clinical application with a focus on the preparation of PMMA-based cement containing bioactive inorganic nanoparticles.[5,6]

As a major inorganic component of bone, hydroxyapatite (HA) has proven to be osteoconductive and osteoinductive.[7,8] HA, when incorporated in PMMA, can form a direct bond with bone to promote the bioactivity of PMMA-based bone cement after implantation.[9–12] Nanosized HA can be harnessed to improve both the bioactivity and mechanical properties of PMMA-based cements.[13,14] However, the high concentration of HA nanoparticles would aggregate easily in a methyl methacrylate (MMA) suspension before polymerization, and this would deteriorate interfacial strength between the HA and PMMA matrix and, consequently, decrease the mechanical properties of PMMA-based cements.[15] One of the effective approaches for this is the modification of the surface of the HA nanoparticles to prevent aggregation. As an effective method, γ-methacryloxypropyl trimethoxysilane (MPS) has been introduced to modify the surface of HA nanoparticles and strengthen the interaction between inorganic and organic compounds.[16,17]

In this study, the surface of HA nanoparticles was modified with poly(methyl methacrylate-*co*-γ-methacryloxypropyl timethoxysilane) [P(MMA-*co*-MPS); Scheme 1]. Taking advantage of P(MMA-*co*-MPS), we greatly improved both the interaction between the inorganic and organic interface and the stability of the HA nanoparticles in MMA. The presence of the PMMA segment in P(MMA-*co*-MPS) could also improve the dispersion of HA in the MMA monomer. Through this strategy, PMMA bone cement with enhanced bioactivity and improved mechanical

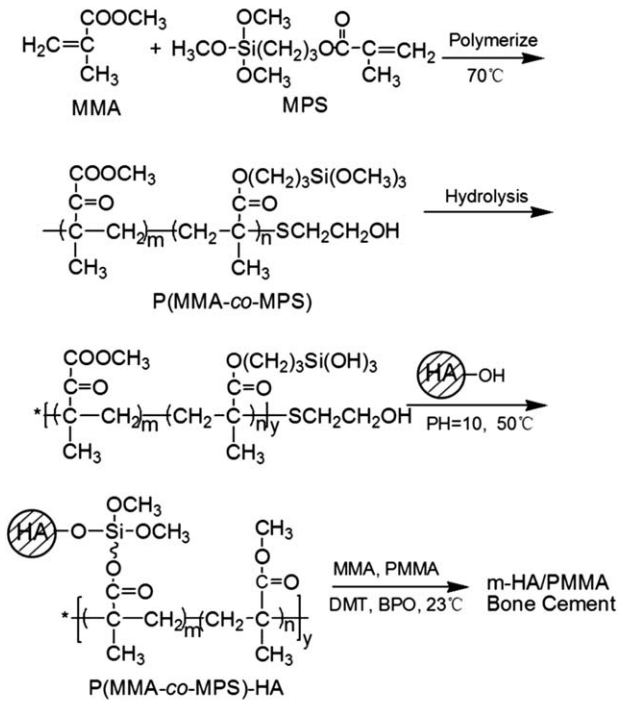

Scheme 1. Preparation of the PMMA-based bone cement containing HA modified by P(MMA-*co*-MPS).

properties were achieved at a high concentration of HA nanofiller, which could be used as a bone repair material in clinical applications.

EXPERIMENTAL

Materials

MMA and poly(ethylene glycol) 2000 (PEG 2000) were purchased from Damao Chemical Reagent Factory (Tianjin, China). MMA was used after distillation under reduced pressure. Poly(vinyl alcohol), benzoyl peroxide (BPO), $(CaNO_3)_2{\cdot}4H_2O$, and $(NH_4)_2HPO_4$ were purchased from Sinopharm Chemical Reagent Co., Ltd. MPS was purchased from Dow Corning (Shanghai, China) and used after distillation under reduced pressure. Dimethyltryptamine (DMT) was purchased from Aladdin Reagent Co. (Shanghai, China) and was used as received. All other reagents were purchased from Guangzhou Chemical Reagent Factory and were used as received.

Synthesis of PMMA

PMMA was synthesized via suspension polymerization with BPO as the initiator. In detail, poly(vinyl alcohol) (0.35 g), MMA (56 mL), and BPO (0.14 g) were dissolved in 360 mL of deionized water. After vigorous agitation for about 1 h at room temperature, the reaction was carried out at 77°C for 2 h. Then, the temperature was adjusted to 87°C and sustained for 2 h. Finally, the temperature of the mixing was increased to 95°C. One hour later, the product was precipitated by distilled water three times, and the final product was dried at 60°C for 48 h *in vacuo*.[18]

Synthesis of P(MMA-*co*-MPS)

P(MMA-*co*-MPS) was synthesized via free-radical polymerization with $HSCH_2CH_2OH$ as the chain-transfer agent. In brief, MMA (12.4148 g), MPS (3.0795 g), 2,2′-azobisisobutyronitrile (0.2036 g), and $SHCH_2CH_2OH$ (0.4499 g) were dissolved in 60 mL of tetrahydrofuran (THF). The solution was purged with nitrogen gas for 1 h at room temperature; then, the reaction was carried out at 70°C for 6 h. The product was precipitated twice in excessive diethyl ether and dried *in vacuo*.[19–22]

Characterization of P(MMA-*co*-MPS) and PMMA

^{1}H-NMR spectra of P(MMA-*co*-MPS) were recorded on a Bruker Avance III spectrometer at 400 Hz with $CDCl_3$ as a solvent.

Gel permeation chromatography (GPC), which was equipped with waters 1515 separations module and waters 2414 refractive index detector, was used to determine the molecular weight of P(MMA-*co*-MPS). The concentration of each copolymer was kept constant at 10 mg/mL, and THF (chromatographic grade) was used as the eluent at a flow rate of 0.3 mL/min.

The viscosity measurements of PMMA were conducted at 25°C in dioxan with an Ubbelohde Schott Geräte automatic dilution viscometer. Both solution samples were prefiltered twice with Swinny stainless Millipore filters (with 1- and 0.45-μm pore sizes).

Synthesis of the HA Nanoparticles

The HA was prepared with poly(ethylene glycol) (weight-average molecular weight = 2000) as a template under ultrasonication. In brief, $(CaNO_3)_2{\cdot}4H_2O$ and $(NH_4)_2HPO_4$ with a molar ratio of 5:3 were dissolved in distilled water. Then, the $(NH_4)_2HPO_4$ solution was added dropwise into the $(CaNO_3)_2{\cdot}4H_2O$ solution under ultrasonication and continuous stirring. The pH of the mixture solutions was adjusted to 10.0 by the addition of $NH_3{\cdot}H_2O$. After the reaction was carried out for 24 h, the mixture was centrifuged at 10,000 rpm. The mixture was refreshed by ethanol and distilled water twice. Then, the product was dried at 60°C for 2 days *in vacuo*.[23]

Surface Modification of HA

The modification of HA was carried out with a solution of MPS in a methanol/water solvent mixture (9:1 v/v). After HA was dispersed in the methanol/water solution, the pH of mixture was adjusted to 3.5–4.0, and then, the P(MMA-*co*-MPS) solution in acetone was added dropwise. The hydrolysis took place in the solution for 60 min at 50°C; 90 min later, the pH was raised to 10.0 with a 10% NaOH solution to promote the condensation reaction. Finally, the products [(P(MMA-*co*-MPS)–HA, abbreviated as modified hydroxyapatite (m-HA)] were filtered with distilled water and washed with THF in an ultrasonic cleaner for 30 min. The final product was dried at 80°C *in vacuo* for 6 h.[24–28]

Characterization of HA and m-HA

The morphology of HA was characterized by transmission electron microscopy (TEM) and field emission scanning electron microscopy (FESEM). At room temperature, a drop of HA suspension (~1.0 mg/mL) was placed on a copper grid with Formvar film and dried before observation on a JEM-1400 TEM at an acceleration voltage of 120 keV.

The calcium content in HA was quantified based on *o*-cresolphthalein complexone according to literature.[29] In brief, *o*-

Table I. Preparation of the PMMA-Based Bone Cements

		Powder			Liquid	
Bone cement	HA (wt %)	PMMA (g)	HA (g)	BPO (g)	MMA (mL)	DMT (μL)
PMMA	0	1.455	0.000	0.045	4.5	10.5
HA/PMMA	5	1.382	0.073	0.045	4.5	10.5
	10	1.310	0.146			
	15	1.237	0.218			
	20	1.164	0.291			
	30	1.019	0.437			
m-HA/PMMA	5	1.382	0.073	0.045	4.5	10.5
	10	1.310	0.146			
	15	1.237	0.218			
	20	1.164	0.291			
	30	1.019	0.437			

cresolphthalein complexone (80 mg), KOH (0.5 mL, 1 mol/L), and acetic acid (1.5 mL) were added to 40 mL of distilled water (defined as solution I). Boric acid (18 g) was added to the mixture composed of 450 mL of ethanolamine and 50 mL of distilled water (defined as solution II). 8-Hydroxyquinoline (8 g) was dissolved in 400 mL of ethanol (defined as solution III). Then, solutions I (5 mL), II (5 mL), and III (1.5 mL) were dissolved in a volumetric flask (100 mL) to prepare the indicator (defined as solution IV). A series of standard Ca^{2+} solutions was prepared within the range of 0–100 μg/mL. Finally, 10 μL of each standard Ca^{2+} solutions and a hydroxyapatite solution (1.0g/ml, dissolved by 0.5M HCL) were put into each well of a 96-well plate. After 300 μL of solution IV was added to each well, the optical density (OD) was measured at 575 nm, which was the wavelength of Ca^{2+} maximum absorption, with a model 550 microplate reader (Bio-Rad), and we calculated the concentration of Ca^{2+} according to the standard curve.

Vanadium–ammonium molybdate colorimetry[30] was introduced to determine the concentration of PO_4^{3-}. Briefly, 0.625 g of ammonium metavanadate and 12.5 g of ammonium molybdate were dissolved in 500 mL of distilled water to prepare the indicator. Volumes of 0, 30, 60, 90, 120, and 150 μL of standard phosphate solutions (50 μg/mL) were added to a 96-well plate. The former indicator (45 μL) was added to each well and diluted to 300 μL. Then, the OD was measured at 355 nm with the model 550 microplate reader (Bio-Rad) for the standard curve. Finally, 100 μL of the PO_4^{3-} solution mentioned previously was added to the 96-well plate. After incubation with the indicator (45 μL) for 15 min at 4°C, the OD was measured at 355 nm, and we calculated the concentration of PO_4^{3-} according to the standard curve.

The crystal structures of HA were characterized with X-ray diffraction (XRD). Wide-angle X-ray scattering characterization was performed with an D/Max-IIIA X-ray diffractometer equipped with a Cu Kα radiation source ($\lambda = 0.154$ nm, 2 kW).

Fourier transform infrared (FTIR) spectroscopy was recorded on a Bruker VERTEX 70 spectrometer. Samples were pressed into potassium bromide pellets.

The content of P(MMA-*co*-MPS) on the surface of HA was determined by thermogravimetric analysis (TGA) and FTIR as an quantitative analysis method.

Preparation of the Bone Cement

Bone cements were prepared by the mixture of solid (powders of HA/m-HA and PMMA) and liquid components (Table I). The ratio between the powder and liquid was 1:1.5 (g:mL). The solid component consisted of PMMA, HA, or m-HA and BPO (initiator). The liquid component contained two compounds: MMA as the monomer and DMT as the polymerization accelerator.

Mechanical Properties of the Composite Bone Cement

According to the ISO5833, the mechanical properties of the composite bone cement samples was tested on a Lloyd universal material testing machine. The samples of the compressive strength test were cast into a cylindrical mold (Length × Diameter: 12 × 6 mm^2). The four-point flexural strength was measured with rectangular samples (Length × Width × Thickness of 75 × 10 × 3.3 mm^3). All of the tests were carried out at crosshead speed of 5 mm/min and a supporting span of 34 mm after they were soaked in phosphate buffer solution (PBS) for 3 days at room temperature. Five duplicates were measured for each sample, and the results were presented as the mean values plus or minus the standard deviation.

Morphology of the Fracture Surface of the Cement

The fracture surface of the cement after the flexural experiment was examined on scanning electron microscope (SEM) with a JSM-6300F instrument. All of the specimens were gold-sputtered. SEM (Quanta 400, Philips) was also used to characterize the surface morphologies of composite bone cement samples after they were soaked in PBS for 3 days.

In Vitro Cytotoxicity Measurement

A 3-(4,5-dimethylthiazol-2-yl)-2,5-diphenyltetrazolium bromide (MTT) assay was carried out to determine the cytotoxicity of the composite bone cement. BALB 3T3 cells were seeded into a 48-well plate (6.0 × 10^4 cells/well) containing 1 mL of DMEM. After incubation for 24 h (37°C, 5% CO_2), the culture medium

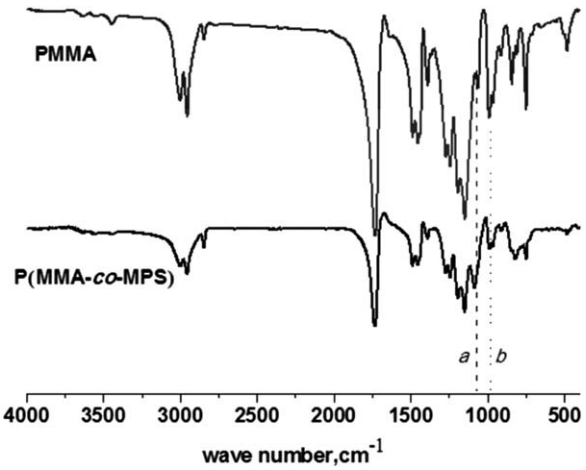

Figure 1. FTIR spectra of PMMA and P(MMA-*co*-MPS).

was removed, and DMEM containing extract of bone cement at particular contents was added to each well. The cells were co-incubated with the extract 37°C for 4 h. Then, the DMEM medium containing extract was replaced by 1 mL of fresh DMEM, and the cells were further incubated at 37°C for 24 and 48 h, respectively. Finally, 60 μL of MTT solution (5 mg/mL) in DMEM was added to each well. After incubation for 4 h, the MTT medium was removed from each well; 200 μL of DMSO was added to each well and incubated in the dark under mild shaking at room temperature for 24 h. The OD was measured at 570 nm on a plate reader (BioTek Synergy4). The cell viable rate was calculated by the following equation:

$$\text{Viable cell } (\%) = (\text{OD}_{\text{treated}}/\text{OD}_{\text{control}}) \times 100$$

where $\text{OD}_{\text{control}}$ was obtained in the absence of the extract and $\text{OD}_{\text{treated}}$ was obtained in the presence of the extract.[31]

RESULTS AND DISCUSSION

Chemical Structure Analysis

The chemical structure of PMMA and P(MMA-*co*-MPS) was confirmed by FTIR spectroscopy. As shown in Figure 1, the absorbance of the symmetric stretching vibrations of C═O occurred at 1732 cm^{-1}, and the stretching vibrations of C—O appeared at 1150 cm^{-1}. The peak at 1081 cm^{-1} was assigned to the bending vibrations of —$SiOCH_3$. Compared with the b peaks in each curve, there was a significant increase in the spectra of P(MMA-*co*-MPS); this indicated the successful preparation of P(MMA-*co*-MPS).

The molecular structure of the obtained P(MMA-*co*-MPS) copolymers were also characterized by ^{1}H-NMR [in Figure 2(a)]. The characteristic peak of MPS appeared at 3.6 ppm [Figure 2(a)], and the peak at 3.75 ppm [Figure 2(d)] can be attributed to the CH_2 [Figure 2(d)] of MPS. As shown in Figure 2(b), the number-average molecular weight of the P(MMA-*co*-MPS) copolymer measured by GPC was about 32,000 g/mol with a polydispersity index (PDI) of 1.41. All of the results indicate that the P(MMA-*co*-MPS) copolymer was successfully synthesized. The molecular weight of PMMA was about 558,000 g/mol as determined by viscometry.

The morphology of HA was visualized by TEM [Figure 3(a)]. The HA nanoparticles exhibited a rodlike shape with a diameter of about 30 nm and a length of about 120 nm. The nanorods were well dispersed as individual particles in distilled water. The morphology of HA was also characterized by FESEM [Figure 3(b)], and the results are in accordance with the morphology determined by TEM.

In the XRD patterns of the HA samples [Figure 3(c)], diffraction peaks corresponding to the HA crystalline phase were found at 2θ angles of 26, 29, 32, 40, and 49°. The presence of an intense diffraction peak at a 2θ angle of 26° revealed the growth of the apatite crystal along the *c* axis. All of the peaks were consistent with The International Centre for Diffraction Data (ICDD) standard card of HA; this indicated that the obtained crystal phase was HA without detectable impurities.[32] The XRD results, in addition to the crystal morphological observation through TEM, support the conclusion that HA was successfully formed.

The Ca/P ratio of the synthetic HA was determined to be 1.756 ± 0.003, which was slightly higher than theoretical value of HA (1.67). This was attributed to the replacement of PO_4^{3-} ions by CO_3^{2-} during the preparation of the HA nanoparticles.

The FTIR spectra were used to confirm the structure of the synthetic HA [Figure 4(a)]. Characteristic peaks of PO_4^{3-} appeared at 1033, 962, 471, 562, and 601 cm^{-1}. The peak at 3575 cm^{-1} was assigned to the stretching vibrations of the hydroxyl group, whereas the peaks at 3440 and 1637 cm^{-1} were related to the bending vibrations of the hydroxyl group in the adsorbed water. The peak at 1410–1460 cm^{-1} might have been due to the absorption of carbon dioxide in the structure of HA, which came from air during the reaction in aqueous medium.

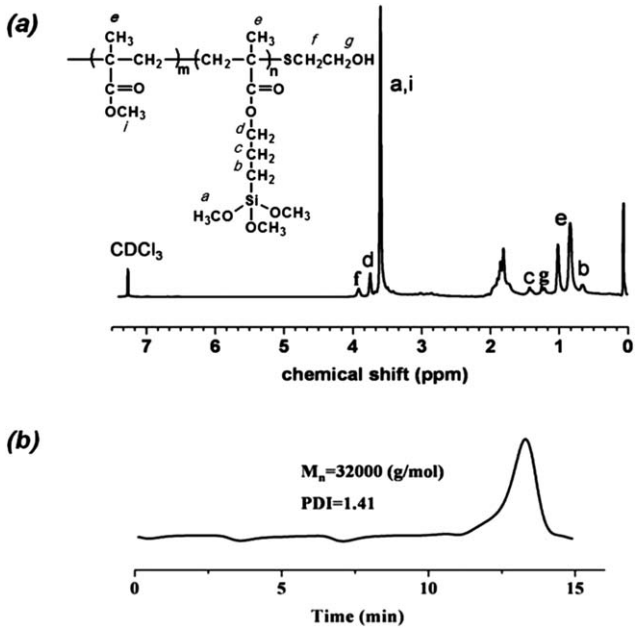

Figure 2. (a) ^{1}H-NMR and (b) GPC spectra of P(MMA-*co*-MPS) (M_n = number-average molecular weight).

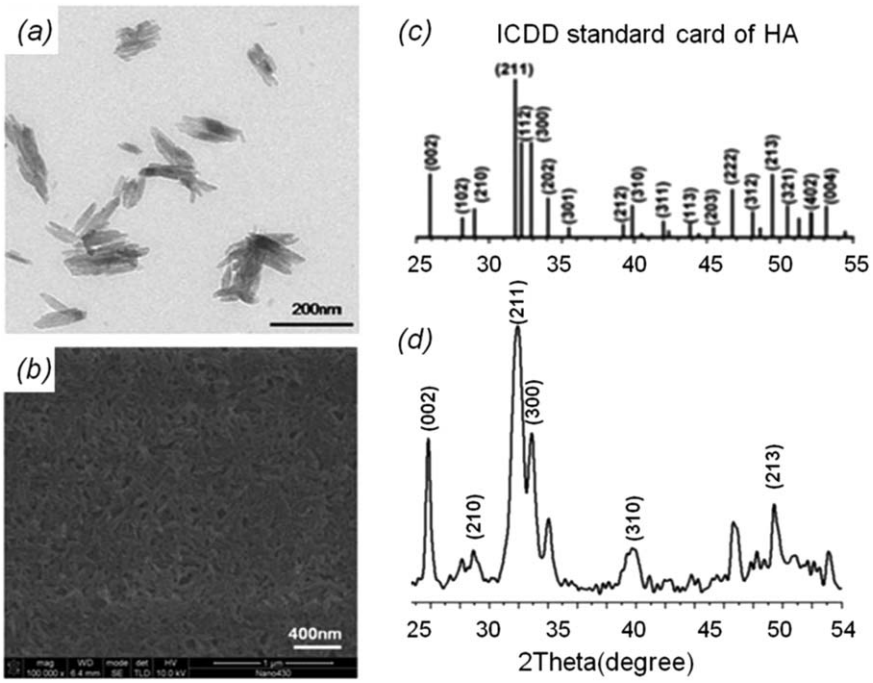

Figure 3. (a) TEM and (b) FESEM images of the HA nanoparticles at 25°C, (c) XRD patterns of the ICDD standard for HA, and (d) XRD patterns of the HA samples.

Compared with that of HA [Figure 4(a)], a new peak occurred at 1732 cm^{-1} in the FTIR spectrum of m-HA; this corresponded to the carbonyl vibrations of C═O in ester bonds, and there was a significant increase in the —CH_3 stretching vibration peak at 3000–2842 cm^{-1}. Additionally, the —OH band at 3440 cm^{-1} disappeared after surface modification with P(MMA-*co*-MPS). This may be attributed to the —OH groups on the HA surface reacting with P(MMA-*co*-MPS) to form Si—O—HA bonds. Moreover, the existence of the hydrophobic PMMA segment could have been another reason for the exclusion of H_2O. All of these results show that surface of HA was successfully modified by P(MMA-*co*-MPS) via covalent bonds.

The amount of P(MMA-*co*-MPS) on the surface of the HA nanoparticles was estimated by TGA. The weight percentage of grafted P(MMA-*co*-MPS) was calculated by the following formula:

$$\text{Weight percentage (wt\%)} = \left(W_{\text{Polymer}} / W_{\text{HA}}\right) \times 100\%$$

where $W_{polymer}$ is the weight loss of P(MMA-*co*-MPS) and W_{HA} is the total weight of the modified HA nanoparticles. As shown in Figure 4(b), when the temperature increased up to 600°C, the m-HA nanoparticles displayed a weight loss of 35.44 wt %; this was ascribed to the decomposition of grafted polymer on the surface of the HA nanoparticles. The data indicate that the P(MMA-*co*-MPS) copolymer was successfully grafted onto the surface of HA.

Mechanical Properties of the Bone Cement

The mechanical properties are one of the most important parameters for the clinical application of bone cement. It is worth mentioning that the molecular weights of PMMA in commercial PMMA bone cement were above 750,000; this made

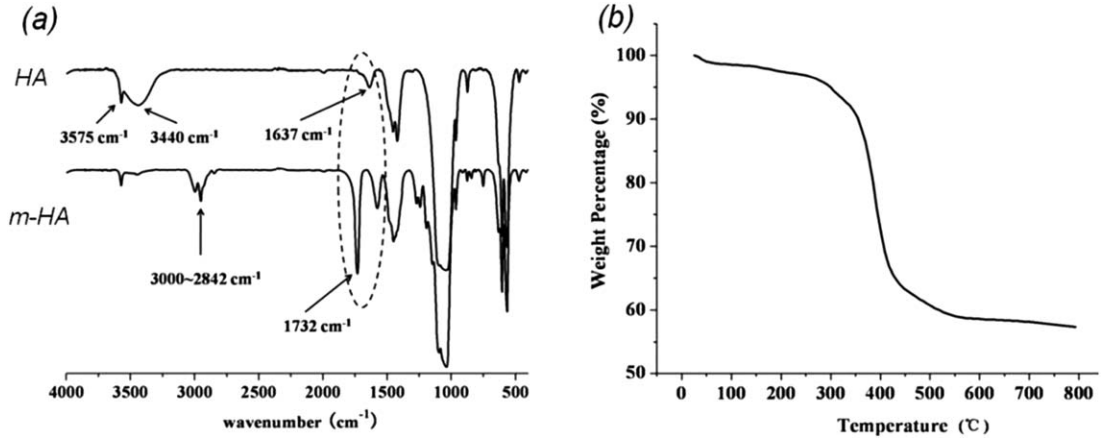

Figure 4. (a) FTIR spectra of the bare HA and HA modified by P(MMA-*co*-MPS) and (b) TGA curve of HA modified by P(MMA-*co*-MPS).

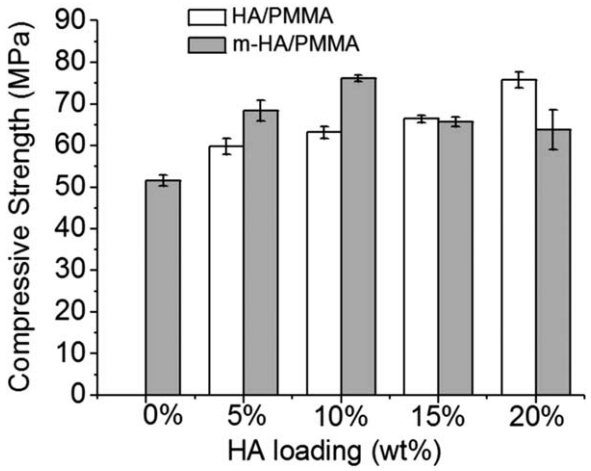

Figure 5. Effect of the HA loading on the compressive strength of PMMA-based bone cement with 5–20 wt % HA (0 wt % is PMMA bone cement).

it difficult to process them during the preparation of cement. In this study, the molecular weight of PMMA used in the obtained cement was about 558,000 g/mol, and m-HA was chosen to reinforce its mechanical properties.

As shown in Figure 5, the compressive strength of the HA/PMMA bone cement containing pristine HA (blank column) increased with the increasing concentration of HA in the cement. The compressive strength of the HA/PMMA bone cement reached about 75 MPa with a concentration of HA in the cement of 20 wt %. This was attributed to the reinforcement effect of HA powders; this improved the compression strength of the PMMA bone cement.

After modification by P(MMA-*co*-MPS), the compressive strength of the m-HA/PMMA cements significantly improved when the content of m-HA was less than 10 wt %. At a concentration of 10 wt %, the compressive strength of the m-HA/PMMA cements reached 76.2 MPa; this was an increase of 47.8% compared with the PMMA bone cement. With the advantage of silane in P(MMA-*co*-MPS), the surface of HA was conjugated with P(MMA-*co*-MPS) by chemical bonding, and the interaction between HA and PMMA was strengthened. This resulted in some microstructural changes and a progressively higher compressive strength during the processing of cements with higher amounts of m-HA particles.

When the content of m-HA was raised up to 20%, the compressive strength of the m-HA/PMMA cements decreased to about 64 MPa. This might have resulted from the aggregation of m-HA in the initial dough of PMMA-based bone cement.[33–35] When the concentration of HA nanoparticles increased, the uniformity of the composite cement became worse, this led to a decrease in the compressive strength. Additionally, to keep the same powder-to-liquid ratio, an increase in the content of the m-HA required a PMMA powder with a lower molecular weight PMMA powder; this, in turn, caused the compressive strength to decrease.

The flexural strength of the cements incorporated with inorganic nanoparticles decreased gradually from 53 to 48 MPa as the proportion of pristine HA [Figure 6(a)] increased up to 20% (blank column). This phenomenon could be attributed to pore formation in the cements through the release of Ca^{2+} ions after soaking. The higher the concentration of HA in the cement was, the lower homogeneity the cement had. Both of these reasons decreased the flexural strength of the cements. However, after the incorporation with HA modified by P(MMA-*co*-MPS), the flexural strength of the m-HA/PMMA cement (gray column) was higher than that of the HA/PMMA cement (blank column) at the same concentration of HA. The flexural strength of m-HA/PMMA increased from 48 to 53.5 MPa when the concentration of HA in the cement was at 20 wt %. All of the results prove that the modification of HA, that is, the strengthening of the interface of HA/PMMA, could effectively suppress the decrease in the flexural strength under physiological conditions.

The flexural modulus of the HA/PMMA (blank column) and m-HA/PMMA (gray column) bone cements increased as the proportion of HA was increased from 5 to 20% [Figure 6(b)]. At 20% HA, the flexural moduli of all of the cements were above 2.10 GPa; this satisfied the requirement of ISO5833. Obviously, the addition of HA nanoparticles enhanced the stiff

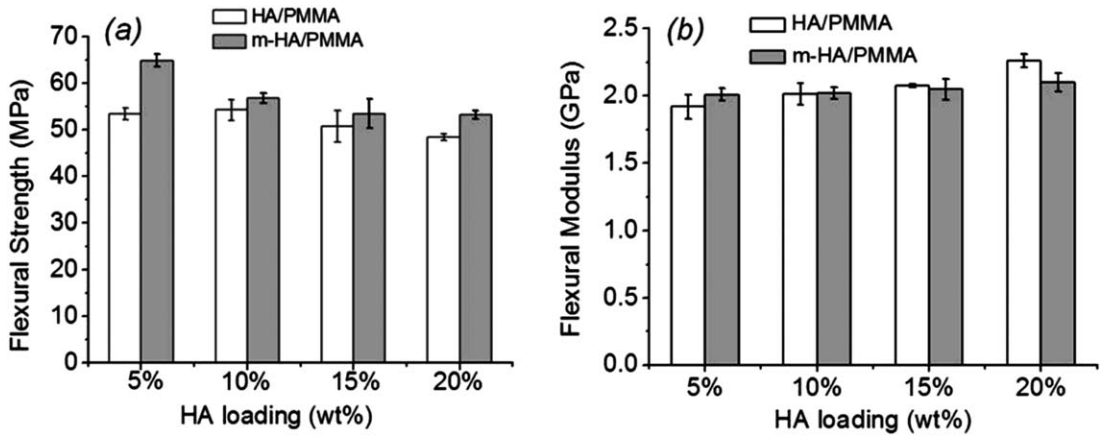

Figure 6. Effect of the HA loading on the (a) flexural strength and (b) flexural modulus of PMMA-based bone cement with 5–20 wt % HA

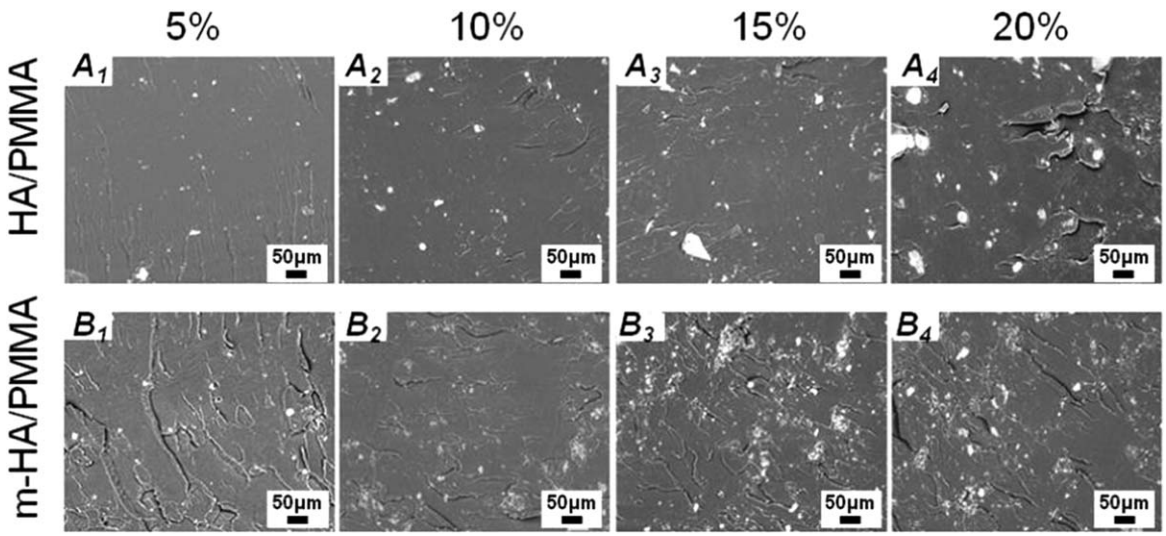

Figure 7. SEM images of the fracture surface of PMMA-based bone cement after the flexural experiment.

structure of the PMMA matrix and improved the flexural modulus of the HA/PMMA bone cement.[36]

As we mentioned previously, the mechanical properties of the PMMA-based bone cement were effectively enhanced by the modification of HA with P(MMA-*co*-MPS), this statement was also supported by the SEM observation of the fracture surface of the composite bone cements. As shown in Figure 7(A), the dispersion of pristine HA in the cross section of the HA/PMMA cements became less uniform with increasing content of HA. In the case of m-HA [Figure 7(B)], the distribution of m-HA in the PMMA matrix was greatly improved, and no large particles were observed; this indicated that the modified HA greatly enhanced their dispersion in the PMMA matrix and made the cement a more uniform composite with improved mechanical properties.

Cytotoxicity

The viability of the BALB 3T3 cells was evaluated to investigate the cytotoxicity of the PMMA cement (Figure 8). It was evident that the viabilities of the BALB 3T3 cells were higher than 85% in the presence of all cements when the content of m-HA in the cements was below 20%. After incubation with m-HA for 48 h, the viability of the cell was higher than that in the first 24 h; this indicated proliferation of the cells. The cell survival rate statistically increased slightly with increasing the content of m-HA. The results indicate that the m-HA/PMMA composite bone cement was of low toxicity and may have potential use in orthopedic applications in the future.

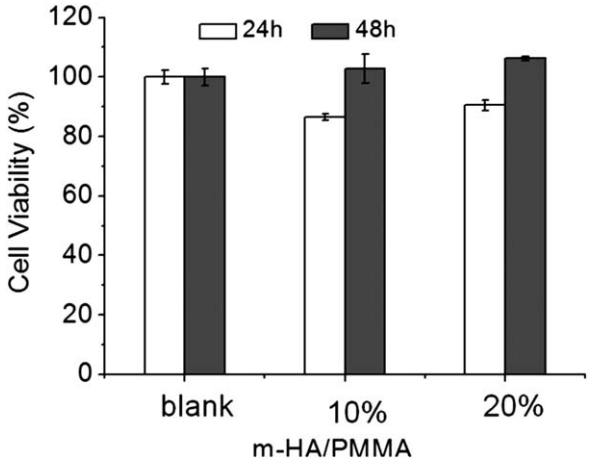

Figure 8. Cell viability of the m-HA/PMMA bone cement (the blank was a cell used as a control).

CONCLUSIONS

HA/PMMA composite bone cements were successfully prepared. After the surface modification of HA by P(MMA-*co*-MPS), the mechanical properties of the PMMA-based bone cements were greatly improved. When the HA mass fraction reached 20%, the compressive strength, flexural strength, and flexural modulus of the cement reached 64, 53, and 2.1 GPa, respectively. The cell viability assay showed that the m-HA/PMMA bone cement was of low toxicity; this indicated that the m-HA/PMMA composite bone cements may be used as bone repair materials on clinical application.

ACKNOWLEDGMENTS

This work was supported by grants from the Ph.D. Programs Foundation of the Chinese Ministry of Education (contract grant number 20110171120008) and the Fundamental Research Funds for the Central Universities (contract grant number 121gpy17).

REFERENCES

1. Kruyta, M. C.; Gaalen, S. M.; Oner, F. C.; Verbout, A. J.; Bruijn, J. D.; Dhert, W. *J. Biomaterials* **2004**, *25*,1463.
2. Charley, J. *Bone Joint Surg.* **1960**, *42*, 28.
3. Liu, Y. K.; Park, J. B.; Njus, G. O.; Stienstra, D. *J. Biomed. Mater. Res.* **1987**, *21*, 247.
4. Harrigan, T. P.; Kareh, J. A.; O'Connor, D. O.; Burke, D. W.; Harris, W. H. A. *J. Orthop. Res.* **1992**, *10*, 134.
5. Lewis, G. *J. Biomed. Mater. Res. B* **1997**, *38*, 155.

6. Mejia, A. G.; Kao, W. H.; Aranda, S. D.; Bastarrachea, M. I. L.; Escamilla, G. C.; Sanchez, F. J. M.; Rodriguez, J. V. C.; Cervantes, J. M. *Mater. Sci. Eng. C* **2013**, *33*, 1737.
7. Fox, K.; Tran, P. A.; Tran, N. *ChemPhysChem* **2012**, *13*, 2495.
8. Ohgushi, H. J.; Caplan, A. I. *J. Biomed. Mater. Res.* **1999**, *48*, 913.
9. Kemal, S.; Korkusuz, F.; Hasirci, N. *Polym. Test.* **2004**, *23*, 145.
10. Woodarda, J. R.; Hilldorea, A. J.; Lanb, S. K.; Parkb, C. J.; Morganb, A. W.; Eurellc, J. A. C.; Clarkd, S. G.; Wheelere, M. B.; Jamisonb, R. D.; Johnson, A. J. W. *Biomaterials* **2007**, *28*, 45.
11. Imaizumi, H.; Sakurai, M.; Kashimoto, O.; Kikawa, T.; Suzuki, O. *Calcif. Tissue Int.* **2006**, *78*, 45.
12. Zhang, J. C.; Liao, J.; Mo, A.; Li, Y. B.; Li, J. D.; Wang, X. *J. Appl. Surf. Sci.* **2008**, *255*, 328.
13. Castaldini, A.; Cavallini, A. *Biomaterials* **1985**, *6*, 50.
14. Gao, H. J.; Ji, B. H.; Jager, I. L.; Arzt, E.; Fratzl, P. *Proc. Natl. Acad. Sci.* **2003**, *100*, 5597.
15. Tham, W. L.; Chow, W. S.; Ishak, Z. A. M. *J. Appl. Polym. Sci.* **2010**, *118*, 218.
16. Simionescu, B.; Olaru, M.; Aflori, M.; Cotofana, C. *High Perform. Polym.* **2010**, *22*, 42.
17. Freris, I.; Cristofori, D.; Riello, P.; Benedetti, A. *J. Colloid Interface Sci.* **2009**, *331*, 351.
18. Ren, L. *Technol. Exp.* **2009**, *123*, 34.
19. Hong, R. Y.; Fu, H. P.; Zhang, Y. J.; Liu, L.; Wang, J.; Li, H. Z.; Zheng, Y. *J. Appl. Polym. Sci.* **2007**, *105*, 2176.
20. Edwin, D. C. L. M.; Carlos, R. *J. Polym. Sci. Part B: Polym. Phys.* **2011**, *49*, 1163.
21. Dan, D.; Mircea, T.; Sever, S.; Liana, F.; Cristian, P. *Eur. Polym. J.* **1999**, *35*, 1679.
22. Wei, H.; Zhang, X. Z.; Cheng, C.; Cheng, S. X.; Zhuo, R. X. *Biomaterials* **2007**, *28*, 99.
23. Sun, X. N.; He, W.; Yan, S. P.; Zhou, W. J.; Han, X. X.; Tian, X. Y.; Han, S. S. *J. Shandong Inst. Light Ind.* **2009**, *23*, 1.
24. Marie, B. S. C.; Makki, A.; Sami, B.; Mohamed, N. B.; Alessandro, G. *J. Colloid Interface Sci.* **2005**, *289*, 249.
25. Dong, H. C.; Ye, P.; Zhong, M. J.; Pietrasik, J.; Drumright, R.; Matyjaszewski, K. *Langmuir* **2010**, *26*, 15567.
26. Wang, S. G.; Zhang, M. C.; Zhong, L. W.; Zhang, W. Q. *J. Mol. Catal. A* **2010**, *327*, 92.
27. Rivera, J. A.; Saldana, J. M.; Bon, R. R. *J. Sol–Gel Sci. Technol.* **2010**, *54*, 312.
28. Li, W. B.; Teng, H.; Qua, J. Q.; Masuda, T. *Prog. Org. Coat.* **2011**, *71*, 376.
29. Yavorskyy, A.; Hernandez-Santana, A.; Shortt, B.; McCarthy, G.; McMahon, G. *Bioanalysis* **2010**, *2*, 189.
30. Yang, H.; Zhang, L. *J. Shananxi Univ. Sci. Technol. (Nat. Sci. Ed.)* **2007**, *25*, 71.
31. Quan, C. Y.; Wu, D. Q.; Chang, C.; Zhang, X. Z.; Zhuo, R. X. *J. Phys. Chem. C* **2009**, *113*, 11262.
32. Li, J. J.; Zhu, D. W.; Yin, J. W.; Liu, Y. X.; Yao, F. L.; Yao, K. D. *Mater. Sci. Eng. C* **2010**, *30*, 795.
33. Morejón, L.; Mendizábal, A. E.; Garcí-Menocal, J. A. D.; Ginebra, M. P.; Aparicio, C.; Mur, M. J. G.; Marsal, M.; Davidenko, N.; Ballesteros, M. E.; Planell, J. A. *J. Biomed. Mater. Res. B* **2005**, *72*, 345.
34. Vallo, C. I.; Montemartini, P. E.; Fanovich, M. A.; Porto López, J. M.; Cuadrado, T. R. *J. Biomed. Mater. Res.* **1999**, *48*, 150.
35. Huang, J. F.; Li, J. Y.; Cao, L. Y.; Zeng, L. P. *J. Appl. Polym. Sci.* **2009**,*116*, 1782.
36. Endogan, T.; Serbetci, K.; Hasirci, N. *J. Appl. Polym. Sci.* **2009**, *113*, 4077.